Research article

Shiqing Li, Zhuo Wang, Shaohua Dong, Sixiong Yi, Fuxin Guan, Yizhen Chen, Huijie Guo, Qiong He, Lei Zhou* and Shulin Sun*

Helicity-delinked manipulations on surface waves and propagating waves by metasurfaces

https://doi.org/10.1515/nanoph-2020-0200
Received March 17, 2020; accepted May 20, 2020

Abstract: Although many approaches have been proposed to manipulate propagating waves (PWs) and surface waves (SWs), usually each operation needs a separate meta-device, being unfavorable for optical integrations. Here, we propose a scheme to design a single meta-device that can *efficiently* generate SWs and/or PWs with pre-designed wavefronts, under the excitations of circularly polarized (CP) PWs with different helicity. As a proof of concept, we design and fabricate a microwave meta-device and experimentally demonstrate that it can convert incident CP waves of opposite helicity to SWs possessing different wavefronts and traveling to opposite directions, both exhibiting very high efficiencies. We further generalize our scheme to design a meta-device and numerically demonstrate that it can either excite a SW beam with tailored wavefront or generate a far-field PW with pre-designed wavefront, as shined by CP waves with different helicity. Our work opens the door to achieving simultaneous controls on far- and near-field electromagnetic environments based on a single ultra-compact platform.

Keywords: far-field; helicity; metasurface; near-field; surface wave.

1 Introduction

Propagating waves (PWs) and surface waves (SWs, electromagnetic (EM) eigen-modes bounded at metal/dielectric interfaces) are two distinct types of EM-wave modes, both having found important applications in practice [1, 2]. The arbitrary control on these two types of EM modes is the vital goal of photonics research. Conventional optical elements (e.g., lenses) utilize the propagating phases accumulated inside the devices to tailor the wavefronts of PWs. Manipulations on surface waves (SWs) have also been achieved by SW devices constructed in the same spirit with optical devices for controlling PWs [3, 4]. However, since natural materials usually exhibit limited variation ranges of permittivity ε and usually do not have magnetic responses (i.e., $\mu = 1$), conventional devices often exhibit curved shapes and bulky configurations to ensure enough phase accumulations, and are usually of low efficiencies due to the impedance-mismatch issue.

Recently, metasurfaces, i.e., ultra-thin metamaterials composed by planar meta-atoms exhibiting tailored phase responses for transmitted or reflected waves, were shown to possess strong capabilities to manipulate EM waves [5–7]. Many fascinating PW-manipulation effects were discovered, including anomalous reflection/refraction [5–8], photonic spin Hall effect [9–11], meta-holograms [12–15], flat lenses [16–23], complex-beam generations [24–28], and many others [29–33]. Meanwhile, gradient metasurfaces were also proposed as new bridges linking PWs and SWs

Shiqing Li and Zhuo Wang are co-first authors.

***Corresponding authors: Shulin Sun**, Shanghai Engineering Research Center of Ultra-Precision Optical Manufacturing, Green Photonics and Department of Optical Science and Engineering, Fudan University, Shanghai, 200433, China; and Academy for Engineering and Technology, Fudan University, Shanghai, 200433, China, E-mail: sls@fudan.edu.cn; and **Lei Zhou**, State Key Laboratory of Surface Physics and Key Laboratory of Micro and Nano Photonic Structures (Ministry of Education), Fudan University, Shanghai, 200433, China; Academy for Engineering and Technology, Fudan University, Shanghai, 200433, China; and Collaborative Innovation Center of Advanced Microstructures, Nanjing, 210093, China, E-mail: phzhou@fudan.edu.cn
Shiqing Li, Shaohua Dong, Sixiong Yi and Yizhen Chen: Shanghai Engineering Research Center of Ultra-Precision Optical Manufacturing, Green Photonics and Department of Optical Science and Engineering, Fudan University, Shanghai, 200433, China
Zhuo Wang, Fuxin Guan and Huijie Guo: State Key Laboratory of Surface Physics and Key Laboratory of Micro and Nano Photonic Structures (Ministry of Education), Fudan University, Shanghai, 200433, China
Qiong He: State Key Laboratory of Surface Physics and Key Laboratory of Micro and Nano Photonic Structures (Ministry of Education), Fudan University, Shanghai, 200433, China; Academy for Engineering and Technology, Fudan University, Shanghai, 200433, China; and Collaborative Innovation Center of Advanced Microstructures, Nanjing, 210093, China

with very high efficiencies [6, 34–36], as long as the variation slopes of reflection/transmission phases on such devices exceed the free-space EM wave-vector. The phase responses of meta-atoms in these metasufaces are dictated by either structural resonances [5, 6] or the Pancharatnam-Berry (PB) mechanism [37, 38], in responses to linearly or circularly polarized (CP) waves, respectively. Utilizing the interfacial effects (e.g., abrupt phase changes) rather than the bulk effects (e.g., propagation phase accumulations), these meta-devices usually exhibit flat configurations, subwavelength sizes, and multiple functionalities. However, while many different schemes have been proposed to manipulate PWs and SWs, usually each of these functionalities needs a separate meta-device, being highly undesired for future integration-optics applications.

In this paper, we propose a new strategy to realize meta-devices that can efficiently and simultaneously manipulate the wavefronts of PWs and SWs in predesigned manners, with functionalities dictated by the helicity of excitation CP wave. As a proof of concept, we first realize a *single* microwave meta-device and experimentally demonstrate that it can convert an input CP PW to a SW beam with wavefront depending on the helicity of excitation CP wave (Figure 1A). We further extend the concept to design another microwave meta-device, which, upon excitations of CP PWs with different helicity, can realize either an anomalously deflected PW or a focused SW, as shown in Figure 1B. Our results substantially enrich the capabilities of metasurfaces to manipulate both far-field and near-field properties of EM waves, which can find many applications in practice.

2 Physical concept

We describe our strategy to design such meta-devices exhibiting multi-functionalities, starting from the functionality of converting a PW to a SW with pre-designed wavefront. As discussed in Ref. [6], to convert a normally incident PW to a SW, we need to construct a metasurface with a linear retardation phase profile $\Phi(x,y) = \Phi_0 + \xi_x x$ where $\xi_x > k_0$ with k_0 being the free-space wave-vector. However, the SW thus generated must exhibit a trivial wavefront with equal-phase planes being *y-z* planes at $x = const$. Now, if we further add a purposely designed $\Psi(y)$ phase function to $\Phi(x, y)$, we can not only generate a SW through the meta-device, but also can simultaneously modulate its wavefront through $\Psi(y)$.

Consider the first case with $\Psi(y)$ varying against y linearly, and then we have

$$\Phi(x, y) = \Phi_0 + \xi_x x + \xi_y y \tag{1}$$

Obviously, shining such a metasurface by a normally incident EM wave, Huygen's law tells us that EM wave reflected must take a tangential **k** vector $\vec{k}_{||} = \xi_x \hat{x} + \xi_y \hat{y}$. In the case of $(\xi_x)^2 + (\xi_y)^2 > k_0^2$, such a "reflected" wave is actually a "driven" SW bounded on the metasurface [6], traveling along an oblique direction in-between x and y axes. To guide such a "driven" SW out of the meta-device, we design a homogeneous "plasmonic metal" supporting an eigen SW mode with wave-vector k_{SW} at this frequency, and then place two pieces of such plasmonic metals at both

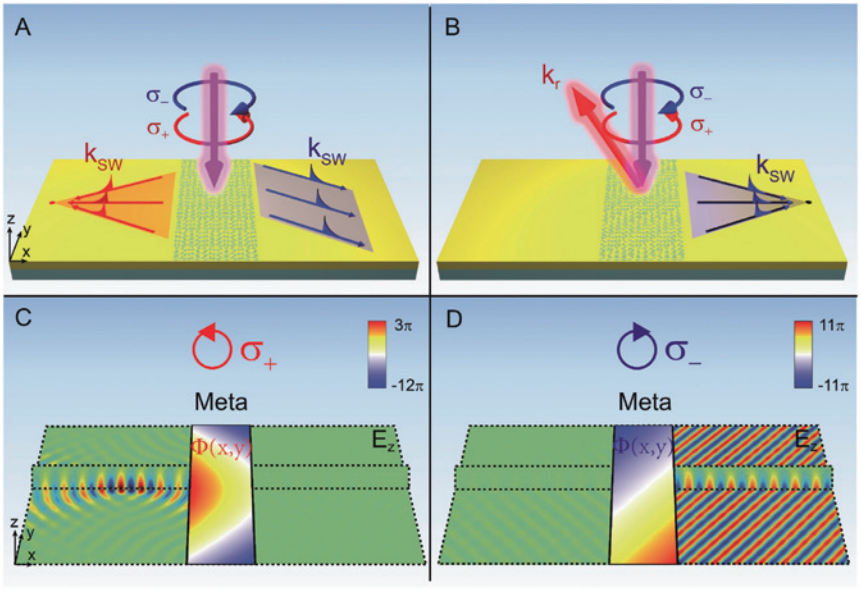

Figure 1: Physical concept and theoretical verifications on ideal models.
Schematics of the proposed metasurfaces to achieve helicity-delinked manipulations on (A) surface waves (SWs) and (B) on both propagating wave (PW) and SW, as shined by circularly polarized (CP) waves of different helicity. Numerically computed Re[E_z] field patterns on the surface of a plasmonic metal supporting an SSP mode with eigen wave-vector k_{SW} at the frequency ω, excited by an ideal current source $\vec{j}(x, y, t) = j_0 \hat{x} \exp[i\Phi(x, y)] \exp(-i\omega t)$ with $\Phi(x, y)$ given by (C) Eq. (3) and (D) Eq. (1), respectively, placed on the top surface of the plasmonic metal. Here, color maps show the distributions of $\Phi(x, y)$.

sides of the meta-device (see Figure 1A). Since k_y must be conserved at the interface between the "plasmonic metal" and the meta-device, the SW generated on the "plasmonic metal" must travel along the direction

$$\theta_r = \sin^{-1}\left(\xi_y / k_{\mathrm{SW}}\right) \tag{2}$$

showing that the SW beam indeed exhibits an oblique equal-phase plane as desired. Full-wave simulations on an ideal model are performed to demonstrate such a scheme, as depicted in Figure 1D (see Sec. A in Supplementary Material for calculation details). In addition, the above argument indicates that the value of ξ_x does not affect the traveling direction (e.g., Eq. (2)) as long as the condition $\sqrt{(\xi_x)^2 + (\xi_y)^2} > k_0$ is satisfied. However, we demonstrate that choosing different ξ_x can slightly influence the final conversion efficiency (see Figure S1 in Supplementary Material). Such a property offers us more freedoms to design our meta-device in practice.

Following this idea, we can generate arbitrary SW beams on the plasmonic metal with desired wavefronts via choosing appropriate $\Psi(y)$ functions. For example, suppose the phase profile is given by

$$\Phi(x, y) = \Phi_0 - \xi_x x - k_{\mathrm{SW}}\left(\sqrt{y^2 + F^2} - F\right) \tag{3}$$

one easily expects that the generate SW beam will focus to a point at a distance F from the device center. Strictly speaking, we need to set an additional restriction on ξ_x to ensure that the generated beam is the SW allowed on the plasmonic metal. Since $\partial\Psi(y)/\partial y$ is not a constant but rather varies from 0 to a finite value as y changes from the middle point to the device edge, we find that a necessary condition is to require that $\xi_x > k_0$, which ensures that no leakage to PW can happen at *every* local point on the meta-device. Finite-element-method (FEM) simulations based on a similar ideal model perfectly demonstrate the desired effect, as depicted in Figure 1C (see Figure S2 in Supplementary Material for more details).

Compared to the SW controls, generating PWs with arbitrary wavefronts are relatively easy to realize, as already demonstrated in previous literature [5, 6, 8]. For example, metasurface with $\Phi(x, y) = \Phi_0 + \xi_y y$ (with $\xi_y < k_0$) can reflect a normally incident PW to an anomalous direction. For other PW-manipulation effects, one can simply retrieve the phase distributions $\Phi(x, y)$ according to the desired functionalities.

Now our strategy is very clear: we need to design a metasurface exhibiting two different reflection-phase distributions in responses to normally incident CP waves with different helicity, as depicted in Figure 1C, D. To achieve this end, we need to find a series of meta-atoms that can possess arbitrary desired phase responses under the excitations of CP waves with different helicity.

3 Meta-atom designs

We choose the microwave regime to prove our scheme. The meta-atoms that we designed are depicted in Figure 2A, which consist of connected-double-ring resonators with arc-length (L) and a metallic ground plane separated by a 3 mm-thick dielectric substrate ($\varepsilon_r = 3 + 0.01i$). Due to the presence of the metallic ground plate, these meta-atoms can completely reflect EM waves polarized along two cross directions (denoted as "u" and "v" axes in the following), but with different reflection phases (φ_{uu} and φ_{vv}). We optimized the geometries of these meta-atoms such that their reflection-phase differences $\varphi_{uu} - \varphi_{vv}$ can remain at about 180° within a quite broad bandwidth (8–18 GHz). As an illustration, we present in Figure 2B the numerically calculated and experimentally measured $\varphi_{uu}(f)$ and $\varphi_{vv}(f)$ spectra of a microwave sample consisting of a periodic array (with periodicity 6 mm) of meta-atoms with L = 3.98 mm. In addition, while varying the arm-length L can change the individual values of $\varphi_{uu}$and φ_{vv}, it does not affect the "half-wave-plate" properties of the resulting meta-atoms, as shown by the calculated $\varphi_{uu} \sim L$ and $\varphi_{vv} \sim L$ relations in Figure 2C at the working frequency 12 GHz. Such broadband half-wave-plate behaviors are obtained by carefully optimizing the anisotropy and quality factors of our meta-atoms.

We now demonstrate that these meta-atoms can provide us the desired helicity-delinked phase responses. Following the Jones' matrix analyses presented in Ref [10], consider one such meta-atom with arc-length L and rotation angle θ with respect to the z axis (see Figure 2A), we find that its spin-flipped (anomalous) reflection coefficient is generally given by $r_a = 0.5 \cdot (r_{uu} - r_{vv}) \cdot e^{i2\sigma\theta}$ with σ denoting the spin of incident CP wave (σ = +: left circular polarization, LCP; σ = −: right circular polarization, RCP). Rewrite the above formula as $r_a = \sqrt{R_a} e^{i\phi_{res}} e^{i\sigma\phi_{PB}} = \sqrt{R_a} e^{i\phi^\sigma}$ with $R_a = |0.5 \cdot (r_{uu} - r_{vv})|^2$ denoting the power efficiency of the anomalous reflection, we find that the total phase of the anomalously scattered wave under CP excitation with spin-σ is

$$\phi^\sigma = \phi_{\mathrm{res}} + \sigma\phi_{\mathrm{PB}} \tag{4}$$

which contains two parts,

$$\begin{cases} \phi_{\mathrm{res}} = \arg(r_{uu} - r_{vv}) \\ \phi_{\mathrm{PB}} = 2\theta \end{cases} \tag{5}$$

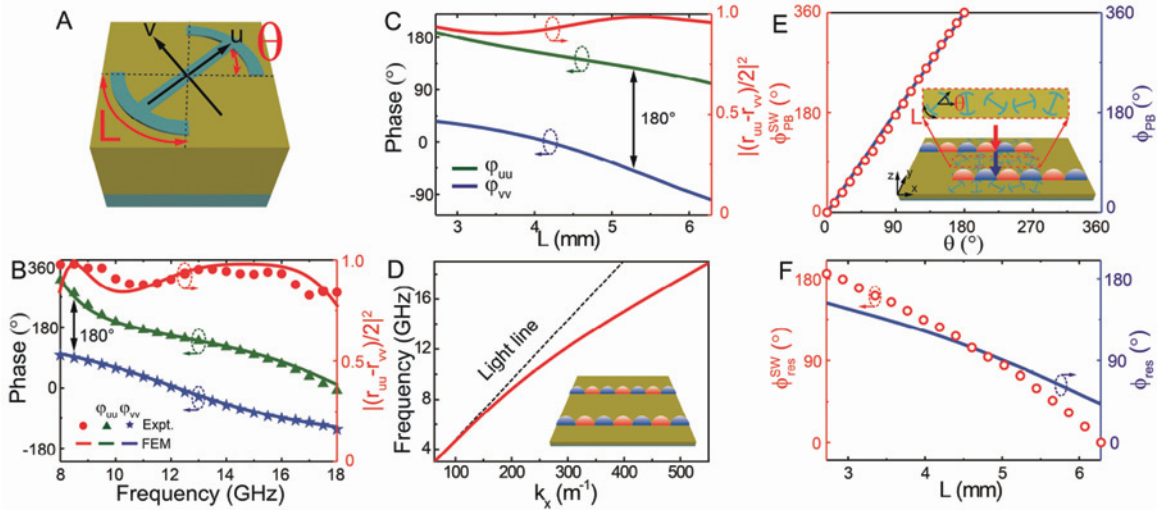

Figure 2: Characterizations on the designed meta-atoms and plasmonic metal.
(A) Geometry of the designed meta-atom (sized 6 × 6mm^2) consisting of a metallic connected-double-ring and a flat metallic mirror separated by a 3 mm thick dielectric spacer. The radius and width of the double-ring are 2.5 and 0.2 mm, respectively. (B) Measured and simulated spectra of reflection-phase (φ_{uu} and φ_{vv}) and working efficiency R_a of the meta-atoms. (C) Reflection phases (φ_{uu} and φ_{vv}) and working efficiency R_a for a series of meta-atoms with different L, obtained by numerical simulations at 12 GHz. (D) Finite-element-method (FEM)-simulated dispersion relation (red line) of the eigen SWs supported by the plasmonic metal as depicted in the inset. (E) Pancharatnam-Berry (PB) phases of meta-atoms with different θ with L fixed at 3.98 mm, obtained by both near-field calculations (see inset) and far-field calculations at 12 GHz. (F) Resonant phases of meta-atoms with different L with θ fixed at 0°, obtained by both near-field calculations (see inset to Figure 2E) and far-field calculations at 12 GHz.

describing, respectively, the phases contributed by the resonance mechanism and the PB mechanism, depending on the structural detail (L) and the orientational angle (θ). Furthermore, since $\phi_{\rm res}$ is independent of spin σ of the incident CP wave while $\sigma\phi_{\rm PB}$ is closely related to σ, the total phases ($\phi_{res} + \sigma\phi_{PB}$) generated by these meta-atoms can thus be controlled *independently* for different spin, which is the desired property. We note that the power efficiencies R_a of these meta-atoms remain at nearly 100% (see Figure 2B, C), implying the excellent performances of the devices fabricated with these meta-atoms.

Solid line in Figure 2F depicts how $\phi_{\rm res}$ changes against L at the frequency 12 GHz, obtained by FEM calculations on a series of periodic metasurfaces consisting of meta-atoms with different L. The $\phi_{\rm res} \sim L$ relation, together with the analytical relation $\phi_{\rm PB} = 2\theta$ presented in Figure 2E, show that varying θ or L can indeed well control the two parts of reflection phases, providing us enough freedoms to design a metasurface exhibiting the desired spin-delinked phase distributions.

We note, however, that these phases ($\phi_{\rm res}$ and $\phi_{\rm PB}$) are obtained by far-field (FF) calculations. Meanwhile, some functionalities being demonstrated here are on SW controls, on which whether these FF phases are still valid remain questionable. To answer this question, we further study the phases of SWs generated by meta-couplers composed by meta-atoms with different L and θ. To begin with, we first design a "plasmonic metal" supporting spoof SWs in the microwave regime, which is a metallic ground plane with a 3 mm-thick dielectric layer put on its top (see inset to Figure 2D). Figure 2D depicts the FEM-simulated dispersion relation of the SW modes supported by such a system, which exhibits an eigen wave-vector $k_{\rm SW} = 1.172k_0$ with k_0 being the free-space wave-vector at the frequency 12 GHz. We next design a series of SW PB meta-coupler composed by a periodic array (periodicity p = 6 mm) of meta-atoms with orientation angles rotating with a step $\Delta\varphi = 50.62°$ along the x axis, generating a dispersionless phase gradient $\xi_x = 2\Delta\varphi/p = 1.172k_0$. Although these meta-couplers all exhibit the same phase gradients, their initial meta-atoms possess different L and θ, thus generating different initial phases. We then connect these meta-couplers with the designed plasmonic metal (see inset to Figure 2E), and then compute the phases of SWs generated on the plasmonic metal, as the meta-couplers are shined by CP waves with σ = + at 12 GHz. Open circles in Figure 2E, F represent the computed SW phases ($\phi_{\rm PB}^{\rm SW}$ and $\phi_{\rm res}^{\rm SW}$) varying against θ and L, respectively. While the computed $\phi_{\rm PB}^{\rm SW} \sim \theta$ relation is strictly identical to the analytical relation (see Figure 2E) protected by the generalized translation invariance symmetry, the $\phi_{\rm res}^{\rm SW} \sim L$ relation, however, exhibits

non-negligible deviations from that obtained with FF calculations (see Figure 2F), indicating that the local-field corrections play very important roles here. Therefore, to get a better performance for our meta-device, we will determine the geometrical parameters (L) of meta-atoms based on the $\phi_{\rm res}^{\rm SW} \sim L$ relation (instead of the original $\phi_{\rm res} \sim L$ relation) when designing meta-devices realizing the SW control functionalities (see Sec. B in Supplementary Material for more details). Obviously, such design scheme is quite different from that for designing metasurfaces achieving helicity-delinked manipulations of free-space waves [39, 40], although based on similar concept. Meanwhile, we still use the original $\phi_{\rm res} \sim L$ relation to sort out the meta-atoms when designing meta-devices for PW-manipulation functionalities.

4 Meta-devices realizations: microwave experiments and simulations

With both near-field and far-field properties of our meta-atoms fully grasped, we now use these meta-atoms to demonstrate two meta-devices with helicity-dependent functionalities. The first meta-device exhibits the following σ-dependent phase distributions at the frequency 12 GHz:

$$\begin{cases} \phi^{+}(x,y) = \phi_0 - \xi_x x - k_{\rm sw}\left(\sqrt{y^2+F^2} - F\right) \\ \phi^{-}(x,y) = \phi_0 + \xi_x x + \xi_y y \end{cases} \tag{6}$$

where $\xi_x = k_{\rm SW} = 1.172k_0$, $\xi_y = -\sin 30° \cdot k_{\rm SW}$ and $F = 120$ mm. According to our analyses presented in Sec. 2, this meta-device can convert two spin-polarized microwaves to SWs flowing to opposite directions, yet exhibiting focusing or deflecting wavefronts. We now employ the meta-atoms designed in Sec. 3 to construct such a meta-device. According to (4), we immediately get the required phase distributions contributed by two mechanisms:

$$\begin{cases} \phi_{\rm res}(x,y) = [\phi^{+}(x,y) + \phi^{-}(x,y)]/2 \\ \phi_{\rm PB}(x,y) = [\phi^{+}(x,y) - \phi^{-}(x,y)]/2 \end{cases} \tag{7}$$

Put Eq. (6) to Eq. (7), we thus obtain the exact values of two phases ($\phi_{\rm res}$ and $\phi_{\rm PB}$) at every point occupied by a meta-atom. Such information, combined with the $\phi_{\rm PB}^{\rm SW} = 2\theta$ and $\phi_{\rm res}^{\rm SW} \sim L$ relations presented in Figures 2E,F, help us unambiguously determine the geometrical sizes (L) and orientation angles (θ) of all meta-atoms located at different positions. Such a strategy guides us to design and fabricate our bi-functional SW metasurface as depicted in Figure 3B

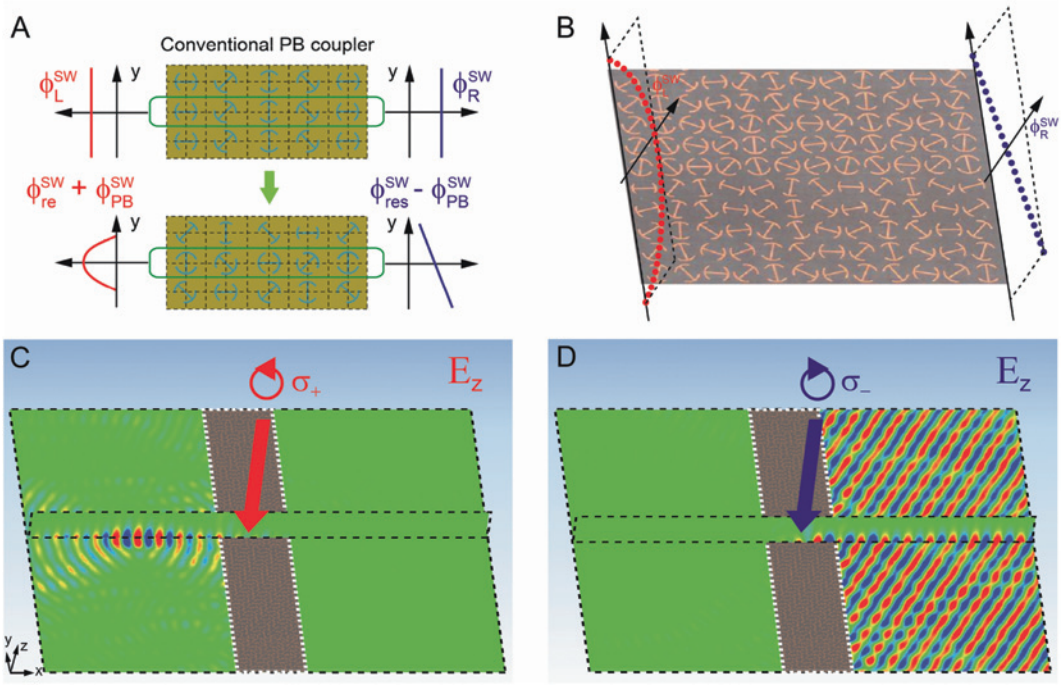

Figure 3: Helicity-delinked metasurface for near-field SW manipulations: numerical demonstrations.
(A) Comparison between a conventional PB meta-coupler and a helicity-delinked bi-functional meta-coupler. (B) Part of the proposed meta-coupler for generating SWs with either hyperbolic or linear phase profile dictated by the helicity of input CP waves. (C, D) FEM simulated near-field Re[E_z] patterns on the whole system, as the meta-coupler is illuminated by CP waves with $\sigma = +$ and $\sigma = -$, respectively.

(see Sec. C in Supplementary Material for more details of the sample). Inside the sample, each column consists of an array of identical meta-atoms with spatially varying θ generating a phase gradient ξ_x, while the initial meta-atoms of different columns are of different L and θ, which collectively generate the desired linear phase profile (blue line) and parabolic phase profile (red line) for CP excitations with different spins.

We first employed FEM simulations to verify our theoretical predictions. Figure 3C, D depict the simulated Re[E_z] field distributions on a reference plane 1 mm above the whole device, as the meta-coupler is shined by normally incident CP waves with different spins. The simulated patterns show clearly that the incident CP waves are first converted into SWs, which are then deflected to an oblique direction (for $\sigma = -$) or focused to a focal point (for $\sigma = +$), respectively. Moreover, the deflection angle is estimated at about 29.5° and the focal length is found as 126.2 mm, both in excellent agreement with theoretical predictions. The efficiencies of two functionalities (i.e., SW anomalous deflection and SW focusing) are estimated as 62% and 61%, respectively. They are lower than the bare efficiencies of individual meta-atoms (Figure 2B, C), due to the following two reasons: 1) The scatterings are enhanced in the process of coupling from PW to SW [34, 42]; 2) Only spoof SWs with transverse-magnetic (TM) polarization exist on the designed "plasmonic metal" while the incident CP wave contains both TM and transverse-electric (TE) components [41]. Such performance can be further improved if a plasmonic metal supporting both TE and TM polarized SWs is adopted in our meta-device. However, we note that these values are already substantially higher than 50% even though the adopted plamonic metal only supports TM SW. This implies that an intriguing polarization cross-talking effect must take place in the conversion process, considering that the impinging CP wave contains 50% TE component and 50% TM component [41].

We finally fabricated out the meta-device and then adopted near-field scanning technique to experimentally characterize its performances. As shown in Figure 4A, we illuminated the meta-coupler by normally incident CP waves emitted from a horn antenna, and then adopted a monopole antenna to map the local Re[E_z] field distribution on a plane 1 mm above the plasmonic metal. Both monopole antenna and horn antenna were connected to a vector network analyzer (Agilent E8362CPNA). Figure 4B–E depict the measured Re[E_z] patterns on the plasmonic metals at two representing frequencies, respectively, as the meta-device is shined by CP waves with different helicity. The measured patterns clearly illustrate the expected helicity-dependent SW manipulations of our meta-device. At the designed working frequency 12 GHz, the measured deflection angle for the SW beam on the right-hand side is $\theta_r = 28.5°$, while the measured focal length of the SW beam on the left-hand side is $F = 131$ mm, in good agreement with both theoretical predictions and full wave simulations (see Figure S6 in Supplementary Material). Interestingly, the meta-device still works well for frequencies slightly deviating away from the working frequency. For example, at 13 GHz, the measured results show clear features of anomalous deflection and focusing effects, although the measured deflection angle (25.5°) and focal length (162 mm)

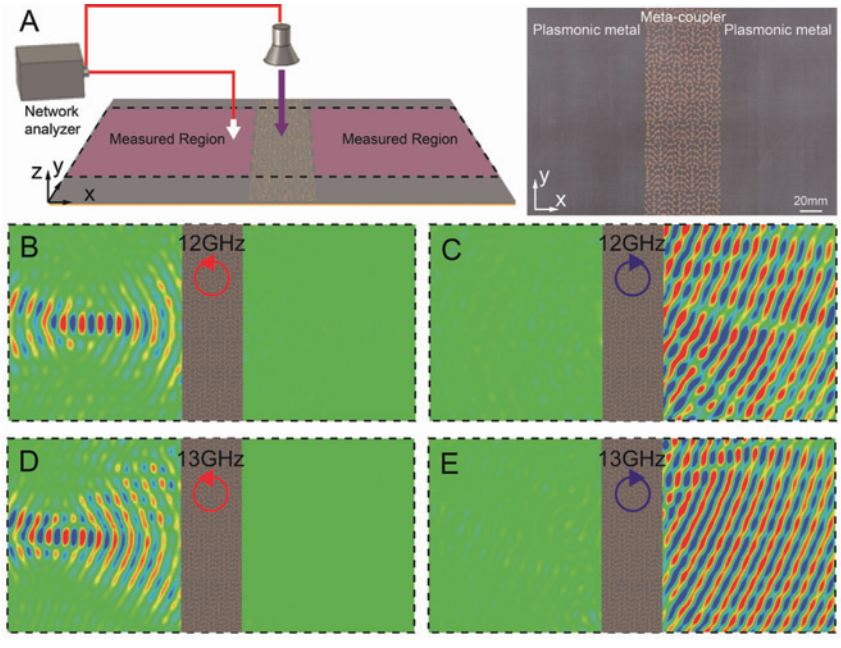

Figure 4: Experimental demonstration on helicity-delinked SW manipulations.
(A) Schematic of the experimental setup consisting of the fabricated PB meta-device connected by two plasmonic metals, a source horn, a monopole detection antenna, and a network analyzer. Right panel in (A) depicts the image of part of the fabricated meta-device sample. Measured Re[E_z] field patterns on the plasmonic metal at (B, C) 12 GHz and (D, E) 13 GHz, as the meta-device is shined by normally incident CP wave with (B, D)$\sigma = +$ and (C, E)$\sigma = -$, respectively.

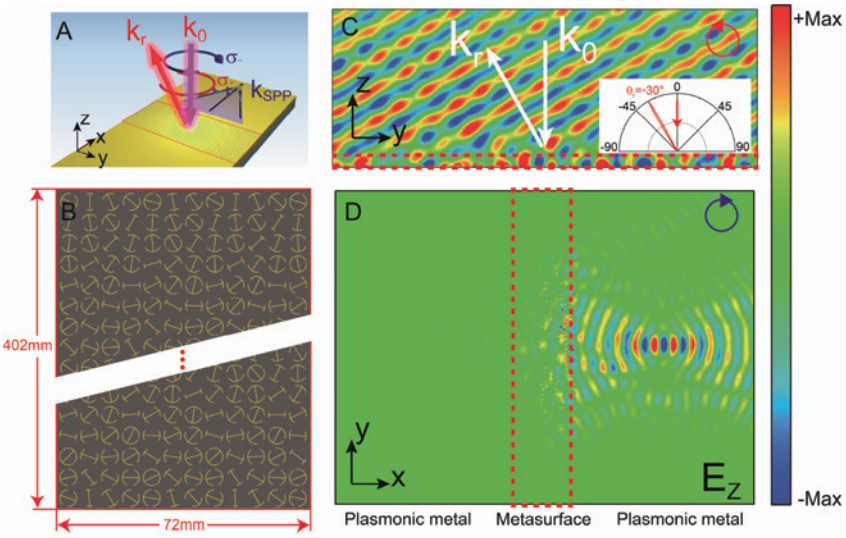

Figure 5: A bi-functional metasurface for both PW and SW manipulations.
(A) Schematic of the designed bifunctional metasurface for simultaneously manipulating PW and SW. (B) Layout of the metasurface composed by PB meta-atoms of different L and θ. (C) Simulated Re[E_z] field pattern on a y-z plane $x = 0$ as the meta-coupler is illuminated by normally incident CP wave with $\sigma = +$. (D) Simulated Re[E_z] field pattern on the top surface of the meta-system as the meta-coupler is illuminated by normally incident CP wave with $\sigma = -$. Here, the working frequency is 12 GHz.

are different from the designed values. In addition, bifunctional metasurface for SW manipulations can operate within a frequency band of about 2 GHz (see Sec. E in Supplementary Material).

We finally employ our scheme to design a meta-device that can achieve helicity-delinked manipulations on both SWs and PWs. We assume that the meta-device exhibits the following helicity-dependent phase distributions at the frequency 12 GHz:

$$\begin{cases} \phi^{+}(x,y) = \phi_0 + \xi_y y \\ \phi^{-}(x,y) = \phi_0 + k_{SW}x - k_{SW}\left(\sqrt{y^2 + F^2} - F\right) \end{cases} \quad (8)$$

where $\xi_y = -k_0 \sin 30°$ and $F = 120$ mm. According to our analyses presented in Sec. 2, we expect that such a meta-device can deflect a normally incident CP beam with $\sigma = +$ to an off-normal direction with $\theta_r = -30°$ on the y-z plane, and can convert a normally incident CP beam with $\sigma = -$ into a SW which is then focused to a point at a distance F away from the device center.

We employ the established strategy to sort out the desired meta-atoms (with appropriate L and θ) for constructing this meta-device. The only difference is that here we used the $\phi_{res} \sim L$ relation obtained by FF calculation (see Figure 2F) to retrieve the geometric parameters L of the meta-atoms. Figure 5B depicts part of the designed sample, with detailed distributions of L and θ given in Figure S8 in Supplementary Material.

We employed numerical simulations to demonstrate the functionality of such a meta-device. Figure 5C depicts the simulated Re[E_z] distribution on a y-z plane with $x = 0$, as the metasurface is illuminated by a normally incident CP with $\sigma = +$. The simulated pattern clearly demonstrates the anomalous reflection functionality of the device for LCP wave. Meanwhile, as we change the helicity of incident CP to $\sigma = -$, we find that now the device first converts the incident CP wave to a SW and then focuses it to a point on the plasmonic metal placed at the right-hand side of the device (see Figure 5D). Finally, we note that the proposed metasurface for SW manipulations still works under small-angle oblique incidences but with efficiencies slightly decreased, as long as the wave-vectors of the "driven" SWs generated on the metasurface do not deviate significantly from that of the eigen SWs on the plasmonic metal (see Sec. G in Supplementary Material for numerical demonstrations).

5 Conclusions

In summary, we proposed a new scheme to employ a single metasurface to simultaneously tailor the wavefronts of SWs and PWs, under the excitations of input CP waves with different helicity. The crucial step is to find a set of meta-atoms exhibiting helicity-delinked phase responses to incident CP excitations, achieved through combining two distinct mechanisms (PB and resonance mechanisms) for phase modulations. As the proof of concept, we employed these meta-atoms to design two meta-devices, and performed full-wave simulations and experiments to demonstrate their excellent helicity-delinked bi-functionalities on wave manipulations. Our results establish a novel platform to control PWs and/or SWs as desired using a single ultra-compact meta-device, which may stimulate many practical applications (e.g., on-chip photonic devices, sensing and super resolution imaging, etc.,) in different frequency regimes.

Acknowledgments: This work was supported by National Natural Science Foundation of China (Nos. 11874118, 11674068, 91850101, 11734007), and National Key Research and Development Program of China (2017YFA0303500, 2017YFA0700201), and Shanghai Science and Technology Committee (Grant No. 18ZR1403400), and Fudan University-CIOMP Joint Fund (FC2018-008, FC2018-006).

Author contribution: All the authors have accepted responsibility for the entire content of this submitted manuscript and approved submission.

Research funding: None declared.

Employment or leadership: None declared.

Honorarium: None declared.

Conflict of interest statement: The authors declare no conflicts of interest regarding this article.

References

[1] H. Raether, *Surface Plasmons on Smooth and Rough Surfaces and on Gratings*. Berlin: Springer; 1988.

[2] W. L. Barnes, A. Dereux, and T. W. Ebbesen, "Surface plasmon subwavelength optics," *Nature*, vol. 424, no. 6950, pp. 824–30, 2003.

[3] A. Hohenau, J. R. Krenn, A. L. Stepanov, et al., "Dielectric optical elements for surface plasmons," *Opt. Lett.*, vol. 30, no. 8, pp. 893–5, 2005.

[4] E. Devaux, J. Y. Laluet, B. Stein, et al., "Refractive micro-optical elements for surface plasmons: from classical to gradient index optics," *Opt. Express*, vol. 18, no. 20, pp. 20610–20619, 2010.

[5] N. Yu, P. Genevet, M. A. Kats, et al., "Light propagation with phase discontinuities: generalized laws of reflection and refraction," *Science*, vol. 334, no. 6054, pp. 333–337, 2011.

[6] S. Sun, Q. He, S. Xiao, Q. Xu, X. Li, and L. Zhou, "Gradient-index meta-surfaces as a bridge linking propagating waves and surface waves," *Nat. Mater.*, vol. 11, no. 5, pp. 426–431, 2012.

[7] X. Ni, N. K. Emani, A. V. Kildishev, A. Boltasseva, and V. M. Shalaev, "Broadband light bending with plasmonic nanoantennas," *Science*, vol. 335, no. 6067, p. 427, 2012.

[8] S. Sun, K. Y. Yang, C. M. Wang, et al., "High efficiency broadband anomalous reflection by gradient meta-surfaces," *Nano Lett.*, vol. 12, no. 12, pp. 6223–6229, 2012.

[9] X. Yin, Z. Ye, J. Rho, Y. Wang, and X. Zhang, "Photonic spin hall effect at metasurfaces," *Science*, vol. 339, no. 6126, pp. 1405–1407, 2013.

[10] W. Luo, S. Xiao, Q. He, S. Sun, and L. Zhou, "Photonic spin hall effect with nearly 100% efficiency," *Adv. Opt. Mater.*, vol. 3, no. 8, pp. 1102–1108, 2015.

[11] W. Luo, S. Sun, H. X. Xu, Q. He, and L. Zhou, "Transmissive ultrathin Pancharatnam-Berry metasurfaces with nearly 100% efficiency," *Phys. Rev. Appl.*, vol. 7, p. 044033, 2017.

[12] G. Zheng, H. Mühlenbernd, M. Kenney, G. Li, T. Zentgraf, and S. Zhang, "Metasurface holograms reaching 80% efficiency," *Nat. Nanotechnol.*, vol. 10, no. 4, pp. 308–312, 2015.

[13] W. T. Chen, K. Yang, C. Wang, et al., "High-efficiency broadband meta-hologram with polarization- controlled dual images," *Nano Lett.*, vol. 14, no. 1, pp. 225–230, 2014.

[14] Z. Deng, J. Deng, X. Zhuang, et al., "Diatomic metasurface for vectorial holography," *Nano Lett.*, vol. 18, no. 5, pp. 2885–2892, 2018.

[15] K. Huang, Z. Dong, S. Mei, et al., "Silicon multi-meta-holograms for the broadband visible light," *Laser Photon. Rev.*, vol. 10, no. 3, pp. 500–509, 2016.

[16] X. Li, S. Xiao, B. Cai, Q. He, T. J. Cui, and L. Zhou, "Flat metasurfaces to focus electromagnetic waves in reflection geometry," *Opt. Lett.*, vol. 37, no. 23, pp. 4940–4942, 2012.

[17] F. Aieta, M. A. Kats, P. Genevet, and F. Capasso, "Multiwavelength achromatic metasurfaces by dispersive phase compensation," *Science*, vol. 347, no. 6228, pp. 1342–1345, 2015.

[18] X. Chen, L. Huang, H. Mühlenbernd, et al., "Dual-polarity plasmonic metalens for visible light," *Nat. Commun.*, vol. 3, pp. 1198, 2012.

[19] M. D. Huntington, L. J. Lauhon, T. W. Odom, "Subwavelength lattice optics by evolutionary design," *Nano Lett.*, vol. 14, no. 12, pp. 7195–7200, 2014.

[20] X. Ding, F. Monticone, K. Zhang, et al., "Ultrathin Pancharatnam-Berry metasurface with maximal cross-polarization efficiency," *Adv. Mater.*, vol. 27, no. 7, pp. 1195–1200, 2015.

[21] W. Pan, T. Cai, S. Tang, L. Zhou, and J. Dong, "Trifunctional metasurfaces: concept and characterizations," *Opt. Express*, vol. 26, no. 13, pp. 17447–17457, 2018.

[22] Q. Wang, X. Zhang, Y. Xu, et al., "A broadband metasurface-based terahertz flat-lens array," *Adv. Opt. Mater.*, vol. 3, no. 6, pp. 779–785, 2015.

[23] P. Anders, G. N. Michael, L. E. René, and I. B. Sergey, "Broadband focusing flat mirrors based on plasmonic gradient metasurfaces," *Nano Lett.*, vol. 13, no. 2, pp. 829–834, 2013.

[24] P. Genevet, N. Yu, F. Aieta, et al., "Ultra-thin plasmonic optical vortex plate based on phase discontinuities," *Appl. Phys. Lett.*, vol. 100, no. 2, p. 013101, 2012.

[25] C. Pfeiffer and A. Grbic, "Controlling vector bessel beams with metasurfaces," *Phys. Rev. Appl.*, vol. 2, p. 044012, 2014.

[26] M. Q. Mehmood, S. Mei, S. Hussain, et al., "Visible-frequency metasurface for structuring and spatially multiplexing optical vortices," *Adv. Mater.*, vol. 28, no. 13, pp. 2533–9, 2016.

[27] Z. Wang, S. Dong, W. Luo, et al., "High-efficiency generation of bessel beams with transmissive metasurfaces," *Appl. Phys. Lett.*, vol. 112, no. 19, p. 191901, 2018.

[28] S. Liu, A. Noor, L. L. Du, et al., "Anomalous refraction and nondiffractive bessel-beam generation of terahertz waves through transmission-type coding metasurfaces," *ACS Photon.*, vol. 3, no. 10, pp. 1968–1977, 2016.

[29] N. Yu, P. Genevet, F. Aieta, et al., "Flat optics: controlling wavefronts with optical antenna metasurfaces," *IEEE J Sel Top Quant. Electron.*, vol. 19, p. 4700423, 2013.

[30] H. T. Chen, A. J. Taylor, and N. Yu, "A review of metasurfaces: Physics and applications," *Rep. Prog. Phys.*, vol. 79, p. 076401, 2016.

[31] S. Sun, Q. He, J. Hao, S. Xiao, and L. Zhou, "Electromagnetic metasurfaces: physics and applications," *Adv. Opt. Photon.*, vol. 11, no. 2, pp. 380–479, 2019.

[32] Q. He, S. Sun, S. Xiao, and L. Zhou, "High-efficiency metasurfaces: principles, realizations, and applications," *Adv. Opt. Mater*, vol. 6, no. 19, p. 1800415, 2018.

[33] F. Ding, A. Pors, S. I. Bozhevolnyi, "Gradient metasurfaces: a review of fundamentals and applications," *Rep. Prog Phys.*, vol. 81, p. 026401, 2018
[34] C. Qu, S. Xiao, S. Sun, Q. He, and L. Zhou, "A theoretical study on the conversion efficiencies of gradient meta-surfaces," *Europhys. Lett.*, vol. 101, no. 5, p. 54002, 2013.
[35] A. Pors, M. G. Nielsen, T. Bernardin, J. C. Weeber, and S. I. Bozhevolnyi, "Efficient unidirectional polarization-controlled excitation of surface plasmon polaritons," *Light Sci. Appl.*, vol. 3, no. 8, p. e197, 2014.
[36] W. Sun, Q. He, S. Sun, and L. Zhou, "High-efficiency surface plasmon meta-couplers: concept and microwave-regime realizations," *Light Sci. Appl.*, vol. 5, no. 1, pp. e16003, 2016.
[37] N. Shitrit, I. Bretner, Y. Gorodetski, V. Kleiner, and E. Hasman, "Optical Spin Hall Effects in Plasmonic Chains," *Nano Lett.*, vol. 11, no. 5, pp. 2038–2042, 2011.
[38] L. Huang, X. Chen, B. Bai, et al., "Helicity dependent directional surface plasmon polariton excitation using a metasurface with interfacial phase discontinuity," *Light Sci. Appl.*, vol. 2, no. 3, p. e70, 2013.
[39] H. X. Xu, L. Han, Y. Li, et al., "Completely Spin-decoupled dual-phase hybrid metasurfaces for arbitrary wavefront control," *ACS Photon.*, vol. 6, no. 1, pp. 211–220, 2018.
[40] J. P. B. Mueller, N. A. Rubin, R. C. Devlin, B. Groever, and F. Capasso, "Metasurface polarization optics: independent phase control of arbitrary orthogonal states of polarization," *Phys. Rev. Lett.*, vol. 118, no. 11, p. 113901, 2017.
[41] J. Duan, H. Guo, S. Dong, et al., "High-efficiency chirality-modulated spoof surface plasmon meta-coupler," *Sci. Rep.*, vol. 7, no. 1, p. 1354, 2017.
[42] F. Guan, S Sun, S. Xiao, Q. He, and L. Zhou, "Scatterings from surface plasmons to propagating waves at plasmonic discontinuities," *Sci. Bull.*, vol. 64, no. 12, pp. 802–807, 2019.

Supplementary Material: The online version of this article offers supplementary material (https://doi.org/10.1515/nanoph-2020-0200).